THE VELOCITY OF SECOND SOUND NEAR THE LAMBDA POINT

by

DAVID LAWRENCE JOHNSON

B.Sc., The University of British Columbia, 1963

M.Sc., The University of British Columbia, 1967

A THESIS SUBMITTED IN PARTIAL FULFILMENT OF THE REQUIREMENTS FOR THE DEGREE OF DOCTOR OF PHILOSOPHY

in the Department

of

Physics

We accept this thesis as conforming to the required standard

THE UNIVERSITY OF BRITISH COLUMBIA

April, 1969

In presenting this thesis in partial fulfilment of the requirements for an advanced degree at the University of British Columbia, I agree that the Library shall make it freely available for reference and Study. I further agree that permission for extensive copying of this thesis for scholarly purposes may be granted by the Head of my Department or by his representatives. It is understood that copying or publication of this thesis for financial gain shall not be allowed without my written permission.

Department of Physics

The University of British Columbia
Vancouver 8, Canada

Date May 15, 1969

DEDICATED

to my wife

ELIZABETH

whose contribution to education

was twofold

and

without whose help

this work would have been

impossible.

ABSTRACT

Direct measurements have been made of the velocity of second sound in liquid helium over the temperature range $T_\lambda - T$ from 1.3×10^{-2} K to 5×10^{-6} K. Using previously determined relationships for the specific heat, superfluid density, and thermal conductivity near the lambda point, consistency has been demonstrated between the measurements, velocities predicted by superfluid hydrodynamics, and certain scaling law predictions.

TABLE OF CONTENTS

Chapter		Page
I	Introduction and Theory	1
	Introduction	1
	Experiment	3
	The Two Fluid Model	4
	Critical Point Arguments	10
II	Apparatus	19
	Cryogenic Apparatus	19
	Electronics	21
	Second Sound Cavity	23
III	Experimental Procedure	28
	Second Sound Trials	28
	Phase Shift and Dispersion Trial	32
IV	Data Reduction	33
	Extraction of Data from the Charts	33
	Analysis of Probable Errors	35
V	Results and Analysis	38
	Results	38
	Comparison with the Hydrodynamic Theory	38
	Comparison with the Scaling Prediction	43
VI	Conclusions and Discussion	45
	Conclusions	45
	Discussion	46
Glossary of Symbols		49
References and Footnotes		52
Appendix I		55

LIST OF TABLES

Table		Page
I	Physical Quantities near T_c	12

LIST OF FIGURES

Figure		Page
1	(k, ξ^{-1}) Plane	15
2	Cryogenic Apparatus	20
3	Block Diagram of Electronics	22
4	Bolometer Electrode Pattern	25
5	Typical Recorder Trace	29
6	Experimental Results	39
7	Deviation Plot	42

ACKNOWLEDGEMENTS

Dr. M.J.Crooks gave many hours of his time for thought-provoking discussions and helpful supervision of my work, for which I thank him heartily.

I am indebted also to Mr. G.Brooks and Mr. R.Weisbach for their technical assistance, to Mr. C.R.Brown for discussions about wave propagation, and to Senor J.Béjar for assistance with the computer programming.

Dr. G.Ahlers very kindly gave his thermal conductivity data and provided some insights into the problem of critical phenomena.

CHAPTER I. INTRODUCTION AND THEORY

(1) INTRODUCTION

In the two decades preceding this one, a slowly increasing collection of experimental data began to indicate remarkable similarities in physical behaviour near the critical points of some otherwise very dissimilar systems. It was realized that transitions such as:

- the superconducting-normal metal transition,
- the liquid-vapour critical transition of a pure fluid,
- the order-disorder transition of some metallic binary alloys,
- the miscible-immiscible critical point of some binary liquid mixtures,
- the ferromagnetic Curie point and the antiferromagnetic Néel point, and
- the liquid helium lambda point,

all behaved in a qualitatively similar way. This realization, coupled with a rapidly improving experimental technology, led to a recent stimulation of interest in the theoretical and experimental investigation of critical phenomena. Classical critical point theories such as the Landau theory of the second-order phase transition, the van der Waals' equation for a liquid, and the Weiss molecular field theory for a ferromagnet, were found both theoretically and experimentally, to be unsatisfactory very

close to the critical temperature .

It has been known for many years that the temperature dependence of a physical quantity near a critical point may often be described by $(T-T_c)^{\underline{e}}$ where T is the absolute temperature, T_c is the critical temperature, and $\underline{e}$ is a constant "critical exponent". Part of the recent theoretical work has been the development of "scaling laws" which attempt to relate to each other the critical exponents or temperature dependences of different physical quantities. One such theory, applied to liquid helium, predicts a relationship between the velocity of second sound below the lambda point and the thermal diffusivity of the liquid above the lambda point.

Classical hydrodynamic arguments, based on the two-fluid model for liquid helium, lead to an expression for the velocity of second sound in terms of the specific heat of the liquid, and the density of its superfluid component. Experimental measurements of this specific heat and superfluid density had been obtained over a temperature range much closer to the lambda point than the range covered by the existing direct measurements of the second sound velocity.

The above considerations all indicated it would be interesting to measure the magnitude and temperature dependence of the velocity of second sound as close to the lambda point as possible.

(2) EXPERIMENT

The experiment we performed basically consisted of the measurement of second sound resonances, or thermal standing waves, in a parallel plate resonator (called the cavity) immersed in and containing helium II.

The use of resonant amplification to detect and measure second sound is well known.[1-4] In general, the conditions for resonance in a cavity depend on the cavity geometry, the frequency of the waves generated in the cavity, and their velocity in the medium contained within the cavity. The usual technique for second sound measurements has been to fix the temperature (and therefore the second sound velocity) and vary the frequency to search for the different resonance modes. In this experiment, a basically different approach was used in that the frequency was fixed and the temperature was not.

The temperature in this experiment was allowed to drift slowly in time. As a consequence, the second sound velocity in the liquid within the cavity was a slow function of time. Resonances were therefore observed with the frequency and resonator geometry fixed, separated in time due to the time dependence of the second sound velocity in the liquid helium. The exper-

imental difficulties associated with the precise control of the liquid temperature were thus eliminated, or more accurately, were reduced to the problems of precise measurement of temperature. It was felt that with this technique observations of the second sound velocity could be made much closer to the lambda point than had been done in previous experiments.[1-3]

(3) THE TWO FLUID MODEL

Many of the properties of liquid helium below the lambda point may be described in terms of a model which assumes two interpenetrating fluids -- the normal fluid (mass M_n, density ρ_n) and the superfluid (mass M_s, density ρ_s), which may move independently of each other, and which together constitute helium II, (mass $M = M_n + M_s$, density $\rho = \rho_n + \rho_s$).[5]

(a) The Hydrodynamic Equations. A system of hydrodynamic equations for helium II may be deduced from the above model,[6] and three assumptions;

(i) that the superfluid fraction has zero entropy;

(ii) that below some critical velocity the motion of the superfluid is irrotational; and

(iii) that all the conservation laws are valid.

Assumption (ii) is written

$$\text{curl } \vec{v}_s = 0 \ , \qquad \ldots(1)$$

where $\vec{v}_s$ is the superfluid velocity. We define $\vec{j}$, the

momentum/unit volume of the fluid. For small superfluid and normal fluid velocities $\vec{v}_s$ and $\vec{v}_n$, $\vec{j}$ can be expanded in powers of the velocities and to a first approximation (neglecting terms in $\vec{v}^2$)

$$\vec{j} = \rho_s \vec{v}_s + \rho_n \vec{v}_n .$$

The conservation of mass equation is

$$\partial\rho/\partial t + \text{div}\ \vec{j} = 0 . \qquad \ldots(2)$$

The first equation of motion, using the conservation of momentum law, is

$$\partial j_i/\partial t + \partial \Pi_{ik}/\partial x_k = 0 , \qquad \ldots(3)$$
$$i,k = 1,2,3,$$

where the summation is carried out over the twice repeated subscripts, and where x_k are the Cartesian coordinates. Π_{ik} is the momentum flux tensor which for small velocities (neglecting viscous effects) is $\Pi_{ik} = p\delta(i,k) + \rho_n v_{ni} v_{nk} + \rho_s v_{si} v_{sk}$, where p is the pressure, and $\delta(i,k)$ is the Kronecker delta function.

Again assuming no dissipative processes we may write the conservation of entropy equation

$$\partial(\rho S)/\partial t + \text{div}\ \vec{F} = 0 ,$$

where $\vec{F}$ is the entropy flux vector and S is the entropy/unit mass of fluid. As entropy is carried only by the normal fluid, $\vec{F} = \rho S \vec{v}_n$ and

$$\partial(\rho S)/\partial t + \text{div}\ (\rho S \vec{v}_n) = 0. \qquad \ldots(4)$$

The internal energy of an incremental mass of liquid helium is given by

$$dU = TdS - pdV + GdM \qquad ...(5)$$

where V is the specific volume and G is the Gibbs free energy per unit mass. Let the mass of this bit of helium now be increased at constant volume (hence dV = 0) by the addition of particles which carry no entropy (hence dS = 0), that is by the addition of superfluid. Then Eq.(5) becomes dU = GdM and we see that the potential energy per unit mass of the superfluid must be G, and that the acceleration of the superfluid must be

$$d\vec{v}_s/dt = \partial\vec{v}_s/\partial t + (\vec{v}_s \cdot \text{grad})\vec{v}_s = -\text{grad}G. \qquad ...(6)$$

The total Gibbs energy MG of the fluid is the sum of the Gibbs energy $MG_o(p,T)$ of the stationary fluid, and the kinetic energy of the relative motion of the normal and superfluid parts.

$$MG = MG_o + (\vec{P}_n^2/2M_n) , \qquad ...(7)$$

where $\vec{P}_n = M_n(\vec{v}_n - \vec{v}_s)$ is the momentum of the normal fluid with respect to the superfluid. Recalling that the masses and densities of the fluid fractions are related by $M_n = (M_n/M)M = (\rho_n/\rho_n+\rho_s)M$, we now differentiate Eq.(7) with respect to M, obtaining

$$\partial MG/\partial M = G_o - (\rho\vec{P}_n^2/2\rho_n M^2) = G$$

Substituting $\vec{P}_n = M\rho_n(\vec{v}_n - \vec{v}_s)/\rho$ we have

$$G = G_o - (\rho_n/2\rho)(\vec{v}_n - \vec{v}_s)^2 ,$$

and substituting this into Eq.(6) gives

$$\partial v_s/\partial t + (\vec{v}_s \cdot \text{grad})\vec{v}_s = -\text{grad}\{G_o - (\rho_n/2\rho)(\vec{v}_n - \vec{v}_s)^2\}. \qquad ...(8)$$

The term $(\vec{v}_s \cdot \text{grad})\vec{v}_s$ may be rewritten

$$(\vec{v}_s \cdot \text{grad})\vec{v}_s = \tfrac{1}{2}\text{grad}\vec{v}_s^2 - \left[\vec{v}_s \times (\text{curl}\vec{v}_s)\right]. \quad \ldots(9)$$

Substitution of Eq.(9) and Eq.(1) into Eq.(8) gives

$$\partial \vec{v}_s/\partial t + \text{grad}\left\{G_o + (v_s^2/2) - (\rho_n/2\rho)(\vec{v}_n - \vec{v}_s)^2\right\} = 0. \quad \ldots(10)$$

Equations (2), (3), (4), and (10) constitute the system of hydrodynamic equations for helium II.

(b) Linearization of the Hydrodynamic Equations. In deriving the velocities of low amplitude sound, we may assume that $\vec{v}_n$ and $\vec{v}_s$ are small and that ρ, S, p and T exhibit only small fluctuations from their equilibrium values ρ_o, S_o, p_o and T_o. The above equations may then be simplified. Neglecting terms in $\vec{v}^2$ in Eqs.(3) and (10), and taking ρS out of the divergence in Eq.(4) we obtain the following system of linearized hydrodynamic equations for helium II:

$$(\partial\rho/\partial t) + \text{div}\,\vec{j} = 0; \quad \ldots(2)$$

$$(\partial j/\partial t) + \text{grad}\,p = 0; \quad \ldots(11)$$

$$(\partial(\rho S)/\partial t) + \rho S \text{div}\,\vec{v}_n = 0; \quad \ldots(12)$$

$$(\partial v_s/\partial t) + \text{grad}\,G_o = 0. \quad \ldots(13)$$

(c) Calculation of Sound Velocities. We now make use of Eqs.(2) to (13) to calculate the velocities of wave propagation. Differentiating Eq.(2) with respect to time and substituting Eq.(11) we obtain

$$\partial^2\rho/\partial t^2 = \text{div grad}\,p. \quad \ldots(14)$$

The identity

$$\partial S/\partial t \equiv (1/\rho)(\partial(\rho S)/\partial t) - (S/\rho)(\partial\rho/\partial t)$$

on substitution of Eqs.(2) and (12) gives

$$\partial S/\partial t = (S\rho_s/\rho)\,\mathrm{div}(\vec{v}_s - \vec{v}_n). \qquad \ldots(15)$$

The Gibbs free energy is $G_o = U + pV - TS$ whence

$$dG_o = -SdT + Vdp = -SdT + (1/\rho)dp.$$

Rearranging this and taking the gradient we obtain

$$\mathrm{grad}\ p = \rho S\,\mathrm{grad}T + \rho\,\mathrm{grad}G_o.$$

Substituting grad p from Eq.(11) and $\mathrm{grad}G_o$ from Eq.(13) gives

$$\rho_n(\partial(\vec{v}_n - \vec{v}_s)/\partial t) + \rho S\,\mathrm{grad}T = 0. \qquad \ldots(16)$$

Differentiating Eq.(15) with respect to time and substituting Eq.(16) we find

$$\partial^2 S/\partial t^2 = S^2(\rho_s/\rho_n)\ \mathrm{div\ grad}\ T. \qquad \ldots(17)$$

Equations (14) and (17) govern the propagation of waves in helium II.

Our previous assumption of small variations in the thermodynamic observables may be written explicitly $\rho = \rho_o + \rho_v(t)$, $S = S_o + S_v(t)$, $p = p_o + p_v(t)$ and $T = T_o + T_v(t)$ where ρ_o, S_o, p_o, and T_o are independent of time. Under these conditions we may further write

$$p_v = (\partial p/\partial\rho)_S\rho_v + (\partial p/\partial S)_\rho S_v, \text{ and}$$
$$T_v = (\partial T/\partial\rho)_S\rho_v + (\partial T/\partial S)_\rho S_v.$$

Equations (14) and (17) are then rewritten

$$\partial^2\rho_v/\partial t^2 = (\partial p/\partial\rho)_S\nabla^2\rho_v + (\partial p/\partial S)_\rho\nabla^2 S_v, \text{ and} \qquad \ldots(18)$$
$$\partial^2 S_v/\partial t^2 = (\rho_s/\rho_n)S^2\left\{(\partial T/\partial\rho)_S\nabla^2\rho_v + (\partial T/\partial S)_\rho\nabla^2 S_v\right\}, \qquad (19)$$

where ∇^2 is the Laplacian operator.

We now wish to know if it is possible for disturbances in the thermodynamic variables, of frequency ω to propagate as waves in the liquid with velocity u. To determine this we now seek simultaneous solutions of Eqs. (18) and (19) of the form $\rho = \rho_0 + \rho' \exp[i\omega(t-x/u)]$ and $S = S_0 + S' \exp[i\omega(t-x/u)]$. Substitution of these into the above equations leads to

$$(\partial T/\partial \rho)_S (\partial S/\partial T)_\rho \rho' - \{(u/u_2)^2 - 1\} S' = 0, \qquad \ldots(20)$$

$$-\{(u/u_1)^2 - 1\} \rho' + (\partial p/\partial S)_\rho (\partial \rho/\partial p)_S S' = 0, \qquad \ldots(21)$$

where

$$u_1^2 = (\partial p/\partial \rho)_S, \text{ and}$$
$$u_2^2 = (\rho_s/\rho_n) S^2 (\partial T/\partial S)_\rho .$$

The condition for the simultaneous solubility of Eqs. (20) and (21), that the determinant of the coefficients be zero, gives

$$\{(u/u_1)^2 - 1\}\{(u/u_2)^2 - 1\} = (\partial T/\partial \rho)_S (\partial S/\partial T)_\rho (\partial p/\partial S)_\rho (\partial \rho/\partial p)_S$$
$$= (C_p - C_v)/C_p ,$$

where C_p and C_v are the constant pressure and constant volume specific heats of the liquid. Using the fact that $C_p \cong C_v$, we now set $(C_p - C_v)/C_p = 0$. With this approximation we then obtain the two solutions

$$u = u_1 = [(\partial p/\partial \rho)_S]^{\frac{1}{2}} , \qquad \ldots(22)$$

$$u = u_2 = [TS^2 \rho_s/\rho_n C_p]^{\frac{1}{2}} . \qquad \ldots(23)$$

If $u = u_1$, Eq.(21) shows that $S' = 0$, and that to the first order in which we are working the entropy fluctuations vanish. This mode is a travelling wave of density fluctuations under adiabatic conditions, i.e. ordinary

or first sound. If $u = u_2$, Eq.(20) shows that the density fluctuations vanish. This is a travelling wave of entropy fluctuations, and therefore temperature fluctuations, at constant density. This is the mode called second sound.

(4) CRITICAL POINT ARGUMENTS

(a) General Discussion. Recent investigations[7] of critical point phenomena have led to the realization that not only do certain physical properties exhibit rather simple behaviours in the vicinity of a critical point, but that their behaviours are very similar near the critical points of apparently very different phase transitions. Arising from such discoveries is the idea that each phase transition is describable in terms of an order parameter $\overset{*}{p}$. (Particular examples are the magnetization of a ferromagnetic material, the condensate wave function of a superfluid, and the concentration in a binary liquid system). This parameter is a measure of the ordering present in the system, and near the critical point it may undergo large fluctuations with small change in the free energy of the system. The special behaviours of the other physical quantities in the critical region are thought to be related to this large susceptibility to fluctuations.

To describe these fluctuations, a correlation function of the general form

$$C^{*}_{p}(\vec{r}) = \left\langle \left[p^{*}(\vec{r}_1) - \langle p^{*}(\vec{r}_1) \rangle \right] \left[p^{*}(\vec{r}_2) - \langle p^{*}(\vec{r}_2) \rangle \right] \right\rangle ,$$
$$\vec{r} = \vec{r}_1 - \vec{r}_2$$

is used, relating the deviations of the order parameter at point $\vec{r}_1$ from its expectation value there to the deviations at point $\vec{r}_2$. In general, this correlation function is a monotonically decreasing function of $\vec{r}$. As such, criteria may be set up to define a particular value of $|\vec{r}|$ called the correlation length, or range ξ of the correlation function. This correlation length ξ is generally a function of temperature, and divergent near the critical point.

As noted above, many quantities depend on ϵ as $\epsilon^{\underline{e}}$ where $\underline{e}$ is some exponent (called the critical exponent) which is fixed if the sign of ϵ is fixed, and $\epsilon = (T-T_c)/T_c$. Table I lists some of the physical quantities pertinent to this experiment, their expected behaviours, and the conventional notation for their critical exponents.

Recently it has been suggested[8-12] that the critical indices are not independent of each other. Through the use of plausibility arguments and assumptions about the functional forms of thermodynamic observables in the critical region, certain relationships called scaling laws have been proposed between various of the critical exponents. Some of these relationships are subject to experimental verification. It should be noted that none of the scaling laws predict the magnitude of any critical exponent. What they do predict is the relationship

TABLE I

Physical Quantities near T_c

Physical Quantity	Critical Exponent e	Expected Behaviour
Order parameter $\overset{*}{p}$	β	$\langle \overset{*}{p} \rangle = 0, \epsilon > 0$ $\langle \overset{*}{p} \rangle \sim \pm \lvert\epsilon\rvert^{\beta}, \epsilon < 0$
Correlation function $C^{\overset{*}{p}}(\vec{r})$ $\vec{r} = \vec{r}_1 - \vec{r}_2$	η	$C \sim \lvert \vec{r}_1 - \vec{r}_2 \rvert^{-d+2-\eta}$ for a d dimensional system
Correlation length, or range of C. ξ	ν ν'	$\xi \sim \epsilon^{-\nu}, \epsilon > 0$ $\xi \sim \lvert\epsilon\rvert^{-\nu'}, \epsilon < 0$
Superfluid density ρ_s	ζ	$\rho_s \sim \lvert\epsilon\rvert^{-\zeta}, \epsilon < 0$

of one critical exponent to another, usually in the form of a sum involving two or more critical exponents.

Correlation functions $C^{\overset{*}{a}}$ may be defined also for operators or physical quantities $\overset{*}{a}$ <u>other</u> than the order parameter. Halperin and Hohenberg[11] point out that scaling arguments may then be subdivided into static or dynamic scaling depending on whether one assumes time independence or dependence of the correlation function, ($C^{\overset{*}{a}}(\vec{r})$ or $C^{\overset{*}{a}}(\vec{r},t)$), and dynamic scaling into restricted or extended dynamic scaling depending on whether or not <u>only</u> the order parameter correlation function is expected to obey the dynamic scaling laws.

(b) <u>A Specific Prediction concerning Second Sound</u>. In a recent paper[11], Halperin and Hohenberg propose a dynamic scaling hypothesis which leads to a specific prediction that may be tested in this experiment. They note that a dynamic correlation function $C^{\overset{*}{a}}(\vec{r},t)$ for some operator $\overset{*}{a}$, may be Fourier transformed to $C_f^{\overset{*}{a}}(\vec{k},\omega)$ and may in general be written in the form

$$C_f^{\overset{*}{a}}(\vec{k},\omega) = 2\pi \cdot C_f^{\overset{*}{a}}(\vec{k}) \cdot f(\omega/\omega^{\overset{*}{a}}(\vec{k})) \cdot [\omega^{\overset{*}{a}}(\vec{k})]^{-1},$$

where

$$\int_{-\infty}^{+\infty} f(x)dx = 1 ,$$

and where the characteristic frequency $\omega^{\overset{*}{a}}(\vec{k})$ is determined by the constraint

$$\int_{-1}^{+1} f(x)dx = \tfrac{1}{2} .$$

A mental picture of the scaling hypothesis may

be obtained as follows. In Fig. 1 we represent the (k,ξ^{-1}) plane, (where k is the wave number and ξ^{-1} is the inverse correlation length). Three regions may be defined in this plane:

- Region I. $k\xi \ll 1$, $T<T_c$. The macroscopic critical region, or hydrodynamic critical region, below the critical temperature. In this region phenomena occur over distances r large compared with ξ. Hydrodynamic arguments are expected to be valid in this and region III.
- Region II. $k\xi \gg 1$. The microscopic critical region in which phenomena occur over distances r small compared with ξ.
- Region III. $k\xi \ll 1$, $T>T_c$. The macroscopic critical region above the critical temperature.
- The critical point is the line $\xi^{-1} = 0$.

The dynamic scaling hypothesis has as its basic assumption that C_I^{*p} (restricted scaling), or C_I^{*a} (extended scaling) vary smoothly in the (k,ξ^{-1}) plane except at the origin, and that either of these correlation functions is essentially specified by its limiting behaviour in regions I, II, and III. That is to say, if the asymptotic forms of the function in regions I (or III) and II are separately extrapolated to the line L_1 (or L_2) in Fig. 1, defined by $k\xi=1$, $T<T_c$ (or $T>T_c$) the two resulting expressions must agree to within a factor of order unity.

The asymptotic forms C^{aI}, C^{aII}, C^{aIII} are defined as

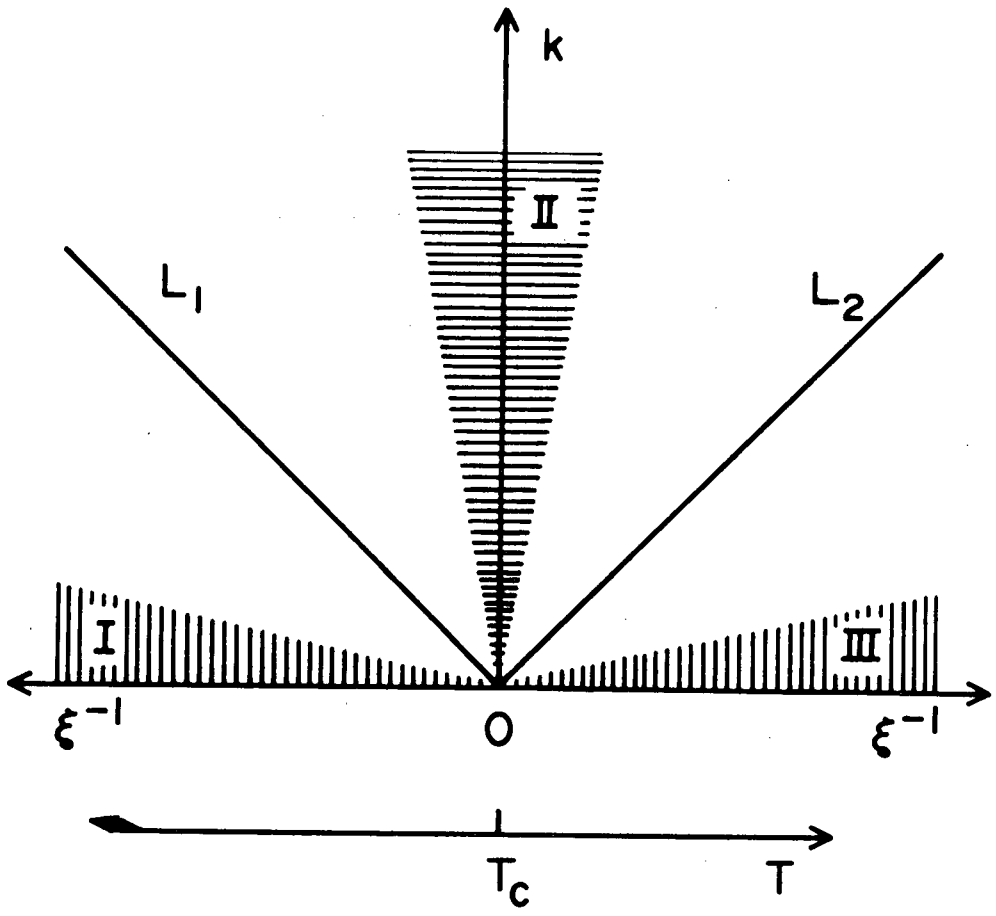

FIGURE 1. The (k, ξ^{-1}) Plane

the limiting forms of $C_f^{\overset{*}{a}}(\vec{k})$ under the conditions:

$$C^{aI} : \xi \text{ fixed, } k \to 0, \; T<T_c ;$$
$$C^{aII} : \xi^{-1} = 0 ;$$
$$C^{aIII} : \xi \text{ fixed, } k \to 0, \; T>T_c .$$

The scaling hypothesis then takes the form of the matching conditions

$$C^{aI}(k) = \alpha C^{aII}(k), \quad \text{for } k = \xi^{-1}$$
$$C^{aIII}(k) = \alpha' C^{aII}(k), \quad \text{for } k = \xi^{-1}$$

whence

$$C^{aIII}(k) = A C^{aI}(k), \quad \text{for } k = \xi^{-1} \qquad \ldots(24)$$

where α, α', A are constants of order unity. Halperin and Hohenberg also propose that similar expressions may be assumed for the characteristic frequencies $\omega^{aI}(k)$, $\omega^{aII}(k)$, $\omega^{aIII}(k)$ in the three regions.

We now consider a particular critical transition, the lambda transition of liquid helium. The critical temperature T_c for this transition is the lambda temperature $T_\lambda = 2.172\,K$, and $\epsilon = (T-T_\lambda)/T_\lambda$.

The specific prediction we will test concerning liquid helium evolves from using as operator $\overset{*}{a}$ the heat operator

$$q(\vec{r},t) = E(\vec{r},t) + (\langle E+p \rangle \cdot \rho(\vec{r},t))/\langle \rho \rangle$$

where $E(\vec{r},t)$ is the energy density of the liquid. Halperin and Hohenberg[11] assume that the heat operator correlation function $C_f^q(\vec{k},\omega)$ shall be dominated in region I ($\epsilon < 0$) by second sound, and in region III ($\epsilon > 0$) by thermal diffusion, and that the asymptotic forms of the

characteristic frequencies in these two hydrodynamic regions may then be derived and are given by

$$\omega^{qI}(\vec{k}) = u_2 k \ , \quad (\epsilon < 0); \qquad \ldots(25)$$

$$\omega^{qIII}(\vec{k}) = D_t k^2 \ , \quad (\epsilon > 0), \qquad \ldots(26)$$

where $D_t = \kappa/\rho C_p$ is the thermal diffusivity of the liquid, and κ is the thermal conductivity. The extended dynamic scaling prediction is then, using Eqs. (24), (25), and (26), the matching condition for $k = \xi^{-1}$ (see lines $k\xi = 1$ in Fig. 1) that

$$D_t \xi^{-2}(\epsilon > 0) = A u_2 \xi^{-1}(\epsilon < 0). \qquad \ldots(27)$$

The two temperature dependent correlation lengths ξ may be written (see Table I) $\xi(\epsilon) = \xi_0 \epsilon^{-\nu}$ and $\xi(-\epsilon) = \xi_0' |-\epsilon|^{-\nu'}$ where ξ_0, ξ_0' are constants. Equation (27) is then rewritten

$$u_2(-\epsilon) = (\kappa(\epsilon)/\rho C_p(\epsilon)) \cdot \left[A \xi_0^2 (\xi_0')^{-1}\right]^{-1} \epsilon^{2\nu} |-\epsilon|^{-\nu'}. \qquad \ldots(28)$$

Now making use of a static scaling law[12]

$$\nu = \nu'$$

and the static scaling assertion[13] that ρ_s is proportional to ξ^{-1} we see that

$$\rho_s \sim |-\epsilon|^{\zeta} \sim \xi^{-1} \sim |-\epsilon|^{\nu'} \ ,$$

and therefore

$$\zeta = \nu' = \nu \ .$$

Experimental measurements[14-16] have shown $\zeta = 0.666 \pm .006 = 2/3$. Thus we obtain for the exponent of ϵ in Eq.(28)

$$2\nu - \nu' = 2/3$$

and Eq.(28) becomes

$$u_2(-\epsilon) = (K(\epsilon)/\rho C_p(\epsilon)) \cdot \left[A\xi_{10}^2 \left(\frac{r'}{r_0}\right)^{-1}\right]^{-1} \epsilon^{2/3}. \qquad \ldots(29)$$

This result was first derived by Ahlers.[17]

CHAPTER II. APPARATUS

(1) CRYOGENIC APPARATUS

The cryogenic apparatus, shown in Fig. 2, consisted of a large outer bath for environmental stability, and a small inner bath containing the second sound cavity. The 3 liter outer bath could be temperature regulated to a short term accuracy of about 10^{-4}K using a Walker diaphragm regulator.[18] The 0.33 liter inner bath was separated from the outer bath on the sides and bottom by a vacuum jacket, and on the top by a 3/8" stainless steel plate. This moderate thermal link gave the inner bath a thermal response time with respect to the outer bath of about one hour. The inner bath was filled from the outer bath through a porous stainless steel filter (to prevent solid nitrogen particles from entering) and a small stainless steel needle valve. The inner bath could be pumped via a pumping line (containing also the electrical leads) terminating in a stainless steel plug bored with a 1 mm diameter hole. Electrical leads were brought through the steel plug by sealing varnish insulated copper wires (AWG #37) into short lengths of stainless steel capillary (1/16" outer diameter, 0.007" inner diameter) using Araldite[19] epoxy. The wires were thus electrically insulated from the steel but the holes in the capillaries were sealed. These cased

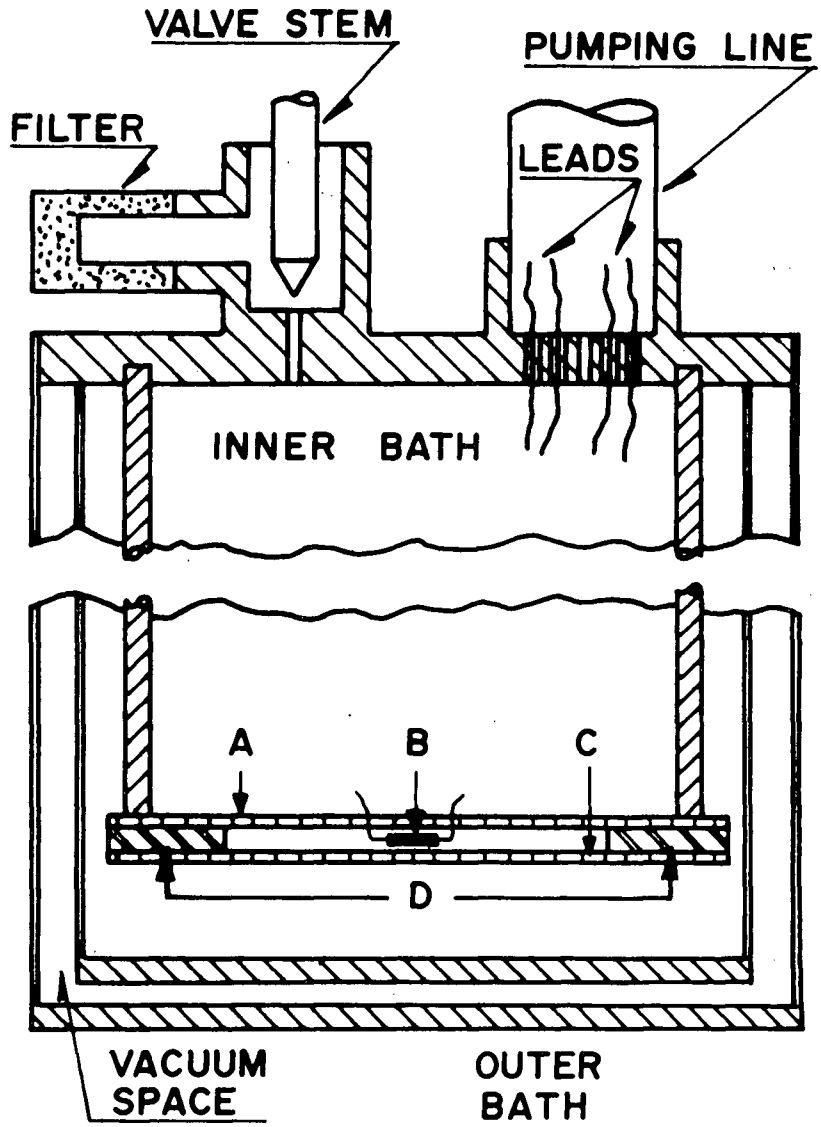

FIGURE 2. Cryogenic Apparatus. A = second sound generator, B = resistance thermometer, C = bolometer, D = Perspex spacers.

wires were sealed with epoxy into 1/16" holes through the plug. Film flow heat transfer between the two baths occurred only through the 1 mm hole, and was therefore small. The second sound cavity, near the bottom of the inner bath, consisted of a 2.5 cm square bolometer separated by 2 mm Perspex spacers from a 2.5 cm square second sound generator (heater). The cavity was oriented horizontally (i.e. second sound propagated vertically) to reduce the gravitationally induced temperature range of the lambda transition[20] to 2.5×10^{-7}K. The cavity was open on two sides. The thermometer, in the center of the cavity, was a carbon resistor.

(2) ELECTRONICS

A block diagram of the electronics is shown in Fig. 3. An oscillator supplied a signal of frequency f/2 to the generator, at which the Joule heating produced a second sound plane wave of frequency f (typically 200Hz to 5KHz) in the liquid. The same f/2 signal, supplied to a frequency doubler, emerged as a signal necessarily coherent with the second sound, and was used as the reference signal for coherent amplifier[21] A (Fig. 3). Thermally induced resistance changes in the bolometer, biased with a constant DC current (ranging from 10 to 30 μA), appeared as voltage changes across the bolometer load resistor which were amplified[22]

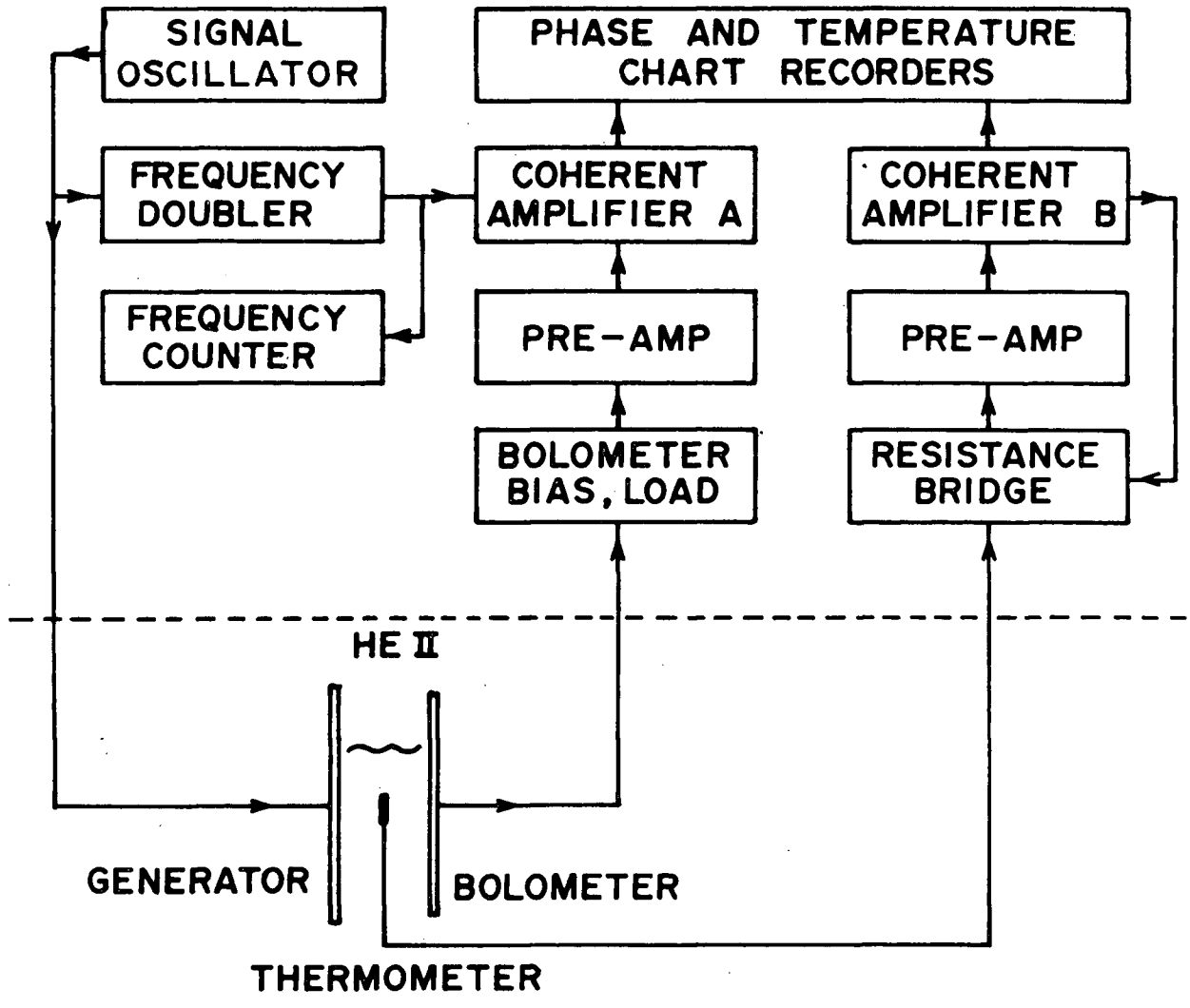

FIGURE 3. Block Diagram of Electronics.

and fed to coherent amplifier A. The output from coherent amplifier A was fed to one channel of a two channel chart recorder.[23] This "second sound trace" was proportional to the product of the second sound amplitude in the cavity and the cosine of the phase of the received second sound with respect to the reference signal.

Coherent amplifier[24] B generated its own reference signal which was also fed to a Wheatstone bridge, one arm of which was the resistance thermometer. The bridge unbalance signal was amplified[25] and fed to coherent amplifier B, the output of which went to the other channel of the chart recorder. This "temperature trace" was proportional to the resistance difference between the thermometer and the preset value of a precision resistance decade.

(3) SECOND SOUND CAVITY

(a) Bolometer. Some desirable properties of a bolometer for second sound detection are:

(i) high thermal sensitivity $(1/R)(dR/dT)$;

(ii) low electrical resistance R to minimize the problems of impedance matching to transmission cables leading out of the cryostat;

(iii) small heat capacity to enable it to respond to very rapid temperature fluctuations; and

(iv) large active area.

The carbon film bolometers constructed by Cannon and Chester[26] exhibit properties (i) and (iii). Significant improvement over their design was achieved using photofabrication techniques rather than thin film evaporation techniques to prepare the bolometer electrodes.

The electrode pattern Fig. 4 was photographically reduced onto Kodak Ortho Type III film. The scale in Fig. 4 represents the final size of the bolometer. A two inch square of 1/16" thick fiberglass was bonded with Araldite[19] epoxy to a 0.001" thick layer of brass. After cleaning with organic solvents in an ultrasonic cleaner, the brass was spray coated with a thin (less than 10^{-4} inch) layer of Kodak KPR photoresist.[27] The photographic negative was contact printed onto the coated brass using ultraviolet light, and the resulting latent image developed. After development, the photoresist has the property that all parts which were exposed to the light become insoluble in most acids, while the unexposed portions dissolve in the developer. The plate was then etched to remove all the brass which was unprotected by developed photoresist. The remaining photoresist was then removed, leaving the pattern of Fig. 4 in 0.001" brass bonded to the fiberglass substrate.

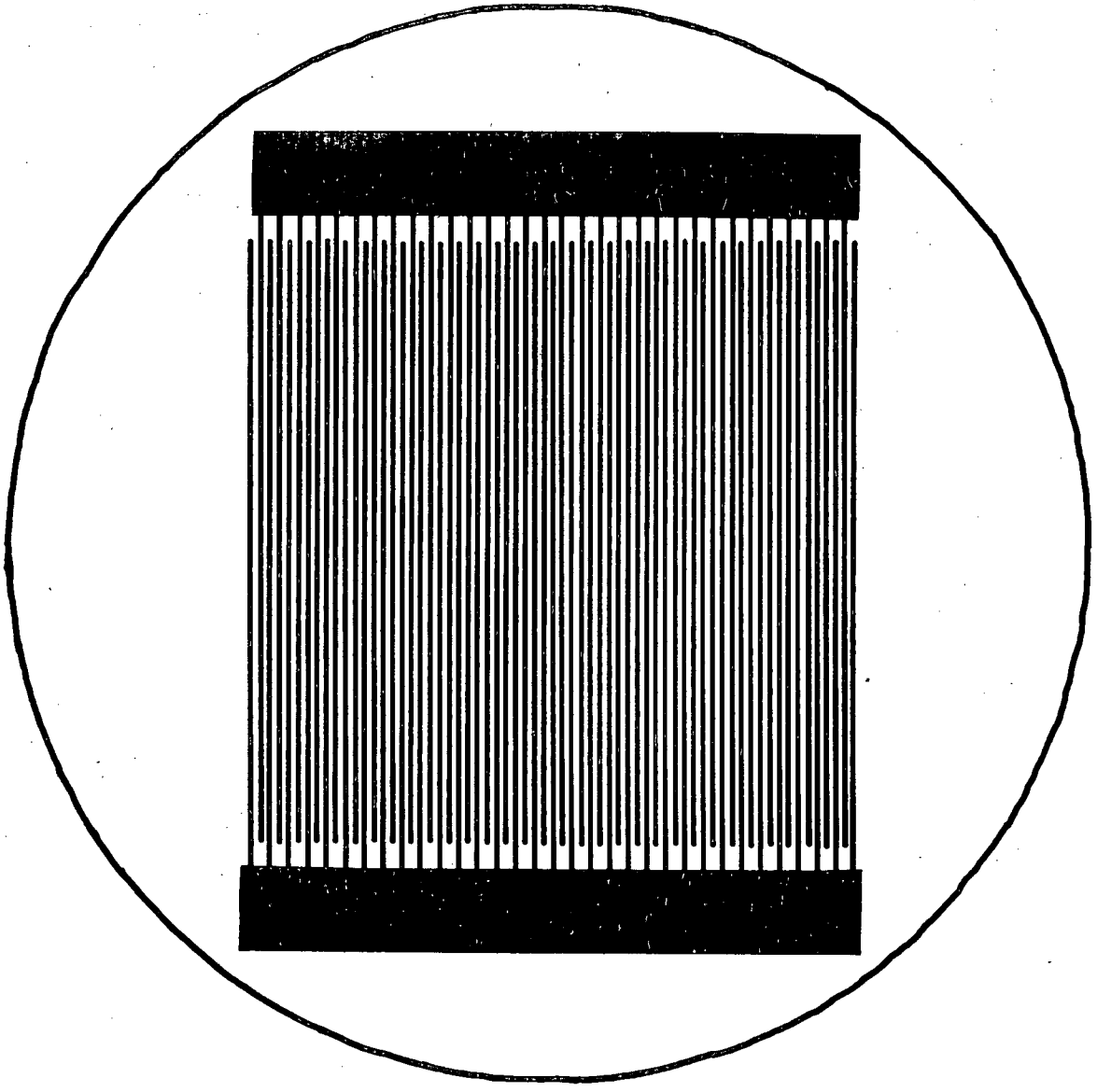

2.5 cm (final size)

FIGURE 4. Bolometer Electrode Pattern.

The bolometer was completed by spraying the prepared electrodes with a suspension of nominally 16 milli-micron carbon particles[28] in xylene. The xylene evaporated leaving an extremely thin layer of semiconducting carbon covering the electrodes. Reference to Fig. 4 will show that the bolometer therefore consisted of 64 thin film carbon resistors wired in parallel, each approximately 2.5 cm wide and 0.02 cm long. Considering the film to be a homogeneous slab of bulk graphite, and using Ohm's law and the measured room temperature resistance, a thickness of 0.1 milli-microns is indicated for the film. As the carbon granules had diameters of the order of 16 milli-microns, one can conclude that the film was microscopically inhomogeneous and roughly the thickness of one carbon granule. This bolometer design achieved the desired properties of low thermal capacity without excessive electrical resistance.

The bolometer resistance and sensitivity while operating at the lambda point were $\sim 70 K\Omega$ and $\sim 3.4\ K^{-1}$ respectively, giving the second sound detection system a maximum sensitivity of $3 \times 10^{-8} K$ rms/chart inch. The maximum temperature wave amplitude observed in the experiment was $10^{-7} K$ rms. Second sound noise (real and

apparent) was less than 3×10^{-9}K rms. The detection system bandwidth was typically 0.25 Hz.

(b) Thermometer. An Allen-Bradley[29] 1/10 watt carbon resistor, nominally 33 ohms at room temperature, was used as the thermometer. Its resistance and sensitivity at the lambda point were $R_\lambda \sim 1200\Omega$ and $(1/R)(dR/dT)_\lambda \sim 1.2\ K^{-1}$ giving the thermometry system a maximum sensitivity of $\sim 10^{-6}$ K/chart inch. Low frequency thermal noise (real and apparent) was about 10^{-6}K peak to peak. The thermal response time of the thermometer was measured in liquid helium and found to be 22 msec at 4.2K and 5 msec at 2.0K.

(c) Second Sound Generator. The second sound generator was a piece of commercial carbon resistance board[30] nominally 25 ohms/square at room temperature. Its resistance at liquid helium temperatures was about 50 ohms/square.

CHAPTER III. EXPERIMENTAL PROCEDURE

(1) SECOND SOUND TRIALS

Data were acquired in the following manner. (Reference will be made to Fig. 5, a typical section of the output from the two channel chart recorder).

(i) With the inner-outer bath valve closed and the outer bath stabilized at a temperature a few millidegrees below T_λ, the inner bath temperature was held steady at $\Delta T \sim 10^{-2}$ to 5×10^{-5}K, where

$$\Delta T = T_\lambda - T.$$

The frequency and coherent amplifier pass-band were set to optimize second sound detection, and the sensitivity (ohms/chart division) of the thermometry system was measured by making discrete changes in the zero setting of the Wheatstone bridge and recording its output.

(ii) With both recording systems and the second sound generator and bolometer operating, pumping of the inner bath was terminated or reduced allowing the temperature to climb slowly up to and through the lambda point, (see Fig. 5 lines #2 and #3), the inner bath dT/dt being typically of the order of 10^{-7} K/sec. The second sound velocity and the temperature were thus functions of time. When velocities occurred such that,

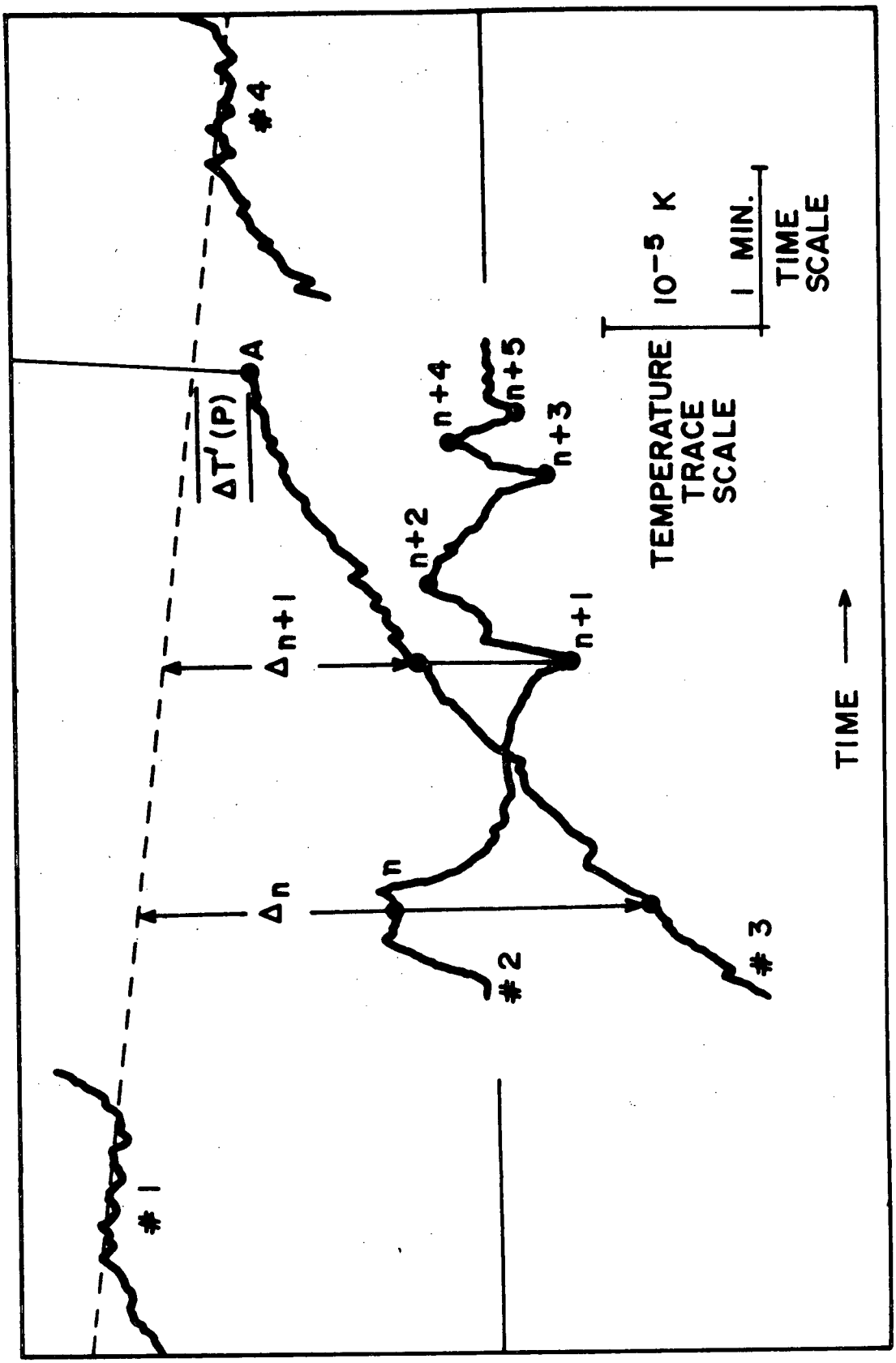

FIGURE 5. Typical Recorder Trace

for the particular frequency in use, the cavity was resonant, peaks were recorded on the second sound trace, (trace #2 in Fig. 5).

(iii) The inner bath temperature was immediately brought slightly below the lambda point, the second sound generator and bolometer were turned off, and the temperature was again allowed to rise through the lambda temperature (see traces #1 and #4 in Fig. 5) to establish R_λ, the thermometer resistance at the lambda point.

Step (iii) was necessary because the accurate identification of the lambda point is dependent on knowing the total power dissipation (P) in the cavity.[16] The combined power input to the cavity from the second sound generator, the bolometer, and the thermometer varied between 25 and 300 microwatts. The thermometer power was 0.1 to 1.0 microwatts. The generator power was always twice the bolometer power so that the DC power inputs (as opposed to the power input at the second sound frequency) of the two were equal, and so that the maximum second sound output signal for a given total power input was obtained. With only the thermometer on, the warming curve (the "temperature trace") showed a zero slope region, or R_λ plateau (traces #1 and #4 in Fig. 5). With the thermometer, generator, and bolometer on, the warming curve broke (point A Fig. 5)

at a temperature $\Delta T'(P)$ slightly below the true lambda temperature and took up a much higher slope dR/dt. $\Delta T'(P)$ was measured and found to be approximately proportional to the total power input P to the cavity. It was assumed that the plateau temperature was the true, or zero power, lambda temperature. If, however, the power dependent shift in the apparent lambda temperature was still in effect during measurements made with the thermometer only, it was $\leq \Delta T'(10^{-6}\ \text{watt}) = 3 \times 10^{-8}\text{K}$.

In previous work,[16,20] a time dependent shift of the lambda point resistance R_λ has been observed. The effect is apparent in the non-zero slope of the R_λ plateaux and of the dashed line in Fig. 5.

The thermometer was calibrated by opening fully the valve between the two baths and measuring thermometer resistance and outer bath vapour pressure for a number of temperatures slightly below T_λ. The data were fitted to the expression $\log R = A + B/T$ which was taken to be exact over the critical region.

Data were extracted from the recorder traces by noting the thermometer resistance R(t) at the time of occurrence of a peak in the second sound trace corresponding to resonance mode n. The experimental second sound velocity was then

$$u_{2e} = 2fd/n, \qquad \ldots(30)$$

(where the subscript e denotes the experimental value for the velocity, and d is the cavity spacing, i.e. the thickness of the Perspex spacers), and the corresponding temperature difference ΔT was a function of $R_\lambda(t)-R(t)$.

(2) PHASE SHIFT AND DISPERSION TRIAL

One run was performed at a fixed $\Delta T \sim 5 \times 10^{-3}$K to determine (a) whether the generator and bolometer were introducing any detectable phase shifts in the second sound signal, (b) whether the cavity had any observable resonance modes other than the axial modes, and (c) whether any dispersion was observable. A search was made from 20 Hz to 5 KHz (covering the range of frequencies used in the experiment) for the second sound resonances. Resonances corresponding to the fifteen axial modes up to this frequency were observed, — and no others. The extrapolated zero frequency phase shift was $0^\circ \pm 15^\circ$, and no departure from linearity in the frequency-phase shift curve was observed. We concluded that (a) at frequencies up to 5 KHz neither the generator nor the bolometer were near their upper frequency response limits, and (b) no dispersion was detectable.

CHAPTER IV. DATA REDUCTION

(1) EXTRACTION OF DATA FROM THE CHARTS.

Line #2 in Fig. 5, the second sound trace, shows the peaks which occurred as the cavity resonated, and contains the velocity information. Lines #1, #3, and #4 contain the temperature information. Data were extracted from the chart as follows.

(i) The zero-power lambda line $R_\lambda(t)$, the dashed line in Fig. 5, was drawn between the R_λ plateaux of two successive traces of the zero power warming curve (#1 and #4 in Fig. 5).

(ii) The relative peak numbers n', $n'+1$, ..., were assigned. The integer n is the mode number of the resonance. It is the number of half wavelengths of second sound in the cavity.

(iii) The distances $\Delta_{n'}$, $\Delta_{n'+1}$, ..., (see Fig. 5) representing $R_\lambda(t) - R(t)$ at the times of occurrence of the peaks n', $n'+1$, ..., were measured, and converted to $\Delta T_{n'}$, $\Delta T_{n'+1}$, using the previously measured sensitivity (ohms/chart division) of the thermometry system and the previously established thermometer calibration R(T).

(iv) The distance of point A (Fig. 5) below the zero-power lambda line was measured and converted to $\Delta T'(P)$, P being the total power used during the recording

of the trace being examined.[31]

(v) The absolute peak number n of the first peak was established. To do this, the second sound velocity had to be known roughly. Equation (30) is rewritten

$$n = 2fd/u_2(\Delta T). \qquad \ldots(31)$$

Taking the measured $\Delta T_{n'}$ for the first peak on the chart, a rough value of $u_2(\Delta T_{n'})$ was inserted into Eq. (31) giving n = real number. This real number, say 3.047, would be within a few percent of some integer. The absolute peak number n was then taken to be that integer.

It should be pointed out that the rough value of $u_2(\Delta T_{n'})$ used to establish n must be erroneous by at least 25% before an error could be incurred in establishing n by this method. Not only must n be an integer, but its parity is known from the direction of deviation of the peak (see Fig. 5) from the center line of the chart. Thus, if the correct n were to be incorrectly identified as n', the error in the value of $u_2(\Delta T_{n'})$ used to establish n' would have had to be at least $\pm 2/(n \pm 2)$. In this experiment the highest value of n for the first peak on a chart was n = 6 giving 25% as the minimum error in $u_2(\Delta T_{n'})$ necessary to produce an incorrect identification of n. As the experimental results will show a maximum deviation of the measured velocity from theory of about 10%, we conclude that no erroneous identifications of n were made.

(vi) The absolute mode numbers of all peaks on the chart having been established via (ii) and (v) the corresponding experimental velocities u_{2e} were calculated using Eq. (30). For each peak recorded on the charts therefore, a data point (u_{2e}, ΔT) has been established and the raw data have been extracted from the charts.

In the course of the experiment 63 charts were measured, producing a total of 276 data points.

(2) ANALYSIS OF PROBABLE ERRORS

(i) Errors in u_{2e}. Error in the absolute velocity can arise from the measurements of f and d (Eq. (30)). As noted above, the error in establishing n is presumed to be zero. The cavity spacing d was determined by measuring the thickness of the Perspex spacers several times with a micrometer and looking at the mean and standard error of the measurements. To obtain the value of d at helium temperatures, the total thermal contraction from room temperature to helium temperature of 1.13%[32] was subtracted giving the low temperature value of $d = 1.913 \times 10^{-3}M \pm 0.6\%$.

The frequency f was measured to $\pm$ 1Hz using a digital counter. The uncertainty in f was therefore 100%/f which was less than 0.5%.

The total probable uncertainty in the absolute value of the measured velocity was therefore taken to

be of the order of 1%.

(ii) Errors in ΔT. The experimental value of ΔT for any point i may be written.

$$\Delta T_i = (B_i)(\Delta_i)\,[f(\Delta_i)]\ ,$$

where B_i is the thermometry system sensitivity (ohms/chart division) for the trace containing point i, Δ_i is the measurement of the temperature trace (chart divisions), and $f(\Delta_i)$ is the resistance thermometer calibration figure in (K/ohm).

The reproducibility of the measurements of B_i depended on the (variable) sensitivity of the system. The probable error in B_i, based on repeated measurements at a fixed temperature, ranged from negligible to about 1%. We therefore take the probable error in B_i to be ± 1%.

The resistance thermometer calibration figure $f(\Delta_i)$ was very nearly a constant equal to $(dT/dR)_\lambda$, the inverse slope of the thermometer resistance vs. temperature calibration curve at the lambda point. As such, its accuracy was determined by the accuracy of the calibration curve, and its probable error is estimated as ± 1%.

Δ_i was obtained by identifying two points on the chart and measuring the distance between them. The probable error involved for each point was arbitrarily

taken to be ±0.03 chart divisions (one inch divisions) and the total uncertainty in Δ_1 was therefore ±0.06 chart divisions giving a total fractional error in Δ_1 of ± ($6/\Delta_1$ chart divisions) %. The values of Δ_1 measured in the experiment ranged from 0.3 to 9.0 chart divisions giving fractional errors of from 20% to 0.7% with an average of about 2%.

The average probable error in the absolute values of the experimental data is therefore taken to be 1% in the velocity u_{2e} and 3% in the temperature difference ΔT.

CHAPTER V. RESULTS AND ANALYSIS.

(1) RESULTS

The experimental results are shown in Fig. 6. The points (u_{2e}, ΔT), (The subscript e denoting the experimental value of the velocity), cover the range $\Delta T = 4.75 \times 10^{-6}$ K to 1.25×10^{-2} K. The temperature differences ΔT and the measured velocities u_{2e} are listed in the first two columns of Appendix I in order of increasing ΔT.

The data overlap the previous measurements of Peshkov[1] ($\Delta T > 10^{-3}$ K), of Pearce, Lipa, and Buckingham[2] (PLB) ($\Delta T > 2 \times 10^{-4}$ K), and of Tyson and Douglass[3] ($\Delta T > 9 \times 10^{-5}$ K). In the ranges of overlap, our data are in excellent agreement with those of Peshkov and of PLB, in both cases well within the experimental uncertainties. In the range $\Delta T = 10^{-4}$ K to 10^{-2} K the Tyson and Douglass measurements give a u_2 which is 5% to 7% low compared to other experimental data, and to the predictions of hydrodynamics.

(2) COMPARISON WITH THE HYDRODYNAMIC THEORY.

The expression for the velocity of second sound,

$$u_{2h} = (TS^2 \rho_s / \rho_n C_p)^{\frac{1}{2}}, \qquad \ldots(32)$$

was derived above using hydrodynamic arguments. We have here used the subscript h to denote this hydrodynamic velocity. Two pieces of experimental work enable one to put Eq. (32) in an analytic form useable in the macroscopic critical region below T_λ. Measurements[14-16] of the superfluid density ρ_s lead to the empirical relation

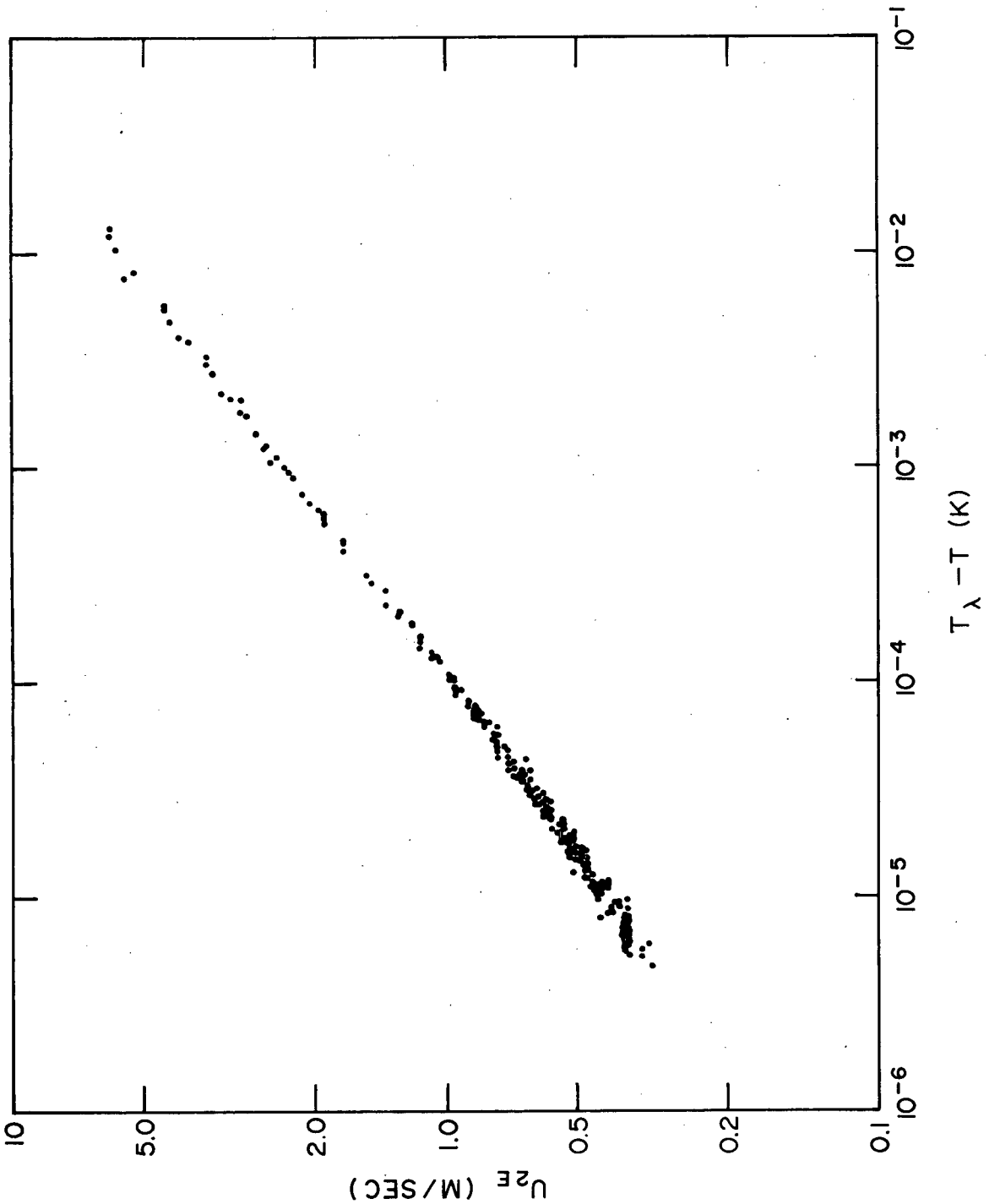

FIGURE 6. Experimental Results.

$$\rho_n/\rho_s = 0.699\Delta T^{-\zeta} - 1 , \qquad ...(33)$$

where $\zeta = 0.666 \pm 1\%$, based on experimental data with $\Delta T \geq 6 \times 10^{-5}$ K. Buckingham, Fairbank, and Kellers' (BFK) measurements[33] of the specific heat are described by the empirical relation

$$C_p = 4.55 - 3.00 \log_{10}|\Delta T| - 5.20\Sigma \ (J/g-K), \qquad ...(34)$$

where $\Sigma = 0$ for $\Delta T > 0$, $\Sigma = 1$ for $\Delta T < 0$, based on experimental data with $|\Delta T| \geq 10^{-6}$ K.

The entropy S of the liquid may be written

$$S(T) = S(T_1) + \int_{T_1}^{T} (C_p/T)dT.$$

Making a change of variable to ΔT, and writing Eq. (34) as $C_p(\Delta T) = A + B\ln\Delta T$ ($\Delta T > 0$) we obtain

$$S(\Delta T) = S(T_1) + A\int_{\Delta T}^{\Delta T_1} \frac{d(\Delta T)}{(T_\lambda - \Delta T)} + B\int_{\Delta T}^{\Delta T_1} \frac{\ln\Delta T \, d(\Delta T)}{(T_\lambda - \Delta T)}. \qquad ...(35)$$

where $\Delta T_1 = T_\lambda - T_1$. Expanding the denominators of Eq. (35) in powers of $\Delta T/T_\lambda$ and neglecting terms of order $(\Delta T/T_\lambda)^2$ we obtain

$$(T_\lambda - \Delta T)^{-1} \cong (1/T_\lambda)(1 + (\Delta T/T_\lambda)) , \qquad ...(36)$$

with a maximum fractional error of 0.1% if $T_1 = 2.10$ K. Substituting Eq. (36) into Eq. (35), performing the integrations, and collecting terms we obtain finally

$$S(\Delta T) = S(T_1) - \qquad ...(37)$$
$$A\ln(T_\lambda - \Delta T_1) + B\left\{(\Delta T_1/T_\lambda)(\ln\Delta T_1 - 1) + \tfrac{1}{2}(\Delta T_1/T_\lambda)^2(\ln\Delta T_1 - \tfrac{1}{2})\right\} +$$
$$A\ln(T_\lambda - \Delta T) - B\left\{(\Delta T /T_\lambda)(\ln\Delta T - 1) + \tfrac{1}{2}(\Delta T /T_\lambda)^2(\ln\Delta T - \tfrac{1}{2})\right\}.$$

We set $T_1 = 2.10$ K, and obtain $S(T_1)$ from the data of Hill and Lounasmaa[34] using their value

$$S(\ 2.10\,K\ ) = 1.24\ (J/g-K). \qquad ...(38)$$

Equation (38) and Eq. (37) with $\Delta T = 0$ give the entropy at the lambda point

$$S(T_\lambda) = 1.55\ (J/g-K).$$

Substitution of Eqs. (33), (34), (37), and (38) into Eq. (32) gives an analytic form for the hydrodynamic velocity of second sound dependent for its accuracy on the validity of the hydrodynamic theory and the extrapolation of Eq. (33) from $\Delta T = 6 \times 10^{-5}\,K$ to $10^{-6}\,K$.

To compare the experimental data with the hydrodynamic theory, a computer was used to evaluate the above mentioned analytic form of u_{2h} using the ΔT from each of the experimental points (u_{2e}, ΔT), and to calculate the ratio

$$R_1(\Delta T) \equiv u_{2e}(\Delta T)/u_{2h}(\Delta T)\ ,$$

for each ΔT. A deviation plot of $\log(R_1)$ against ΔT is shown in Fig. 7, and the corresponding values of $u_{2h}(\Delta T)$ are tabulated in the third column of Appendix I. The mean value of R_1 and its 95% confidence limits are

$$\bar{R}_1 = \langle u_{2e}/u_{2h} \rangle_{av} = 1.000 \pm .004\ . \qquad ...(39)$$

In obtaining the above result we have extrapolated Eq. (33). As a check on the self-consistency of this extrapolation, a weighted least squares fit[35] of the data to the <u>form</u> of Eq. (32) was performed to predict the values of Q and ζ in the expression

$$u_{2e} = (\ TS^2/C_p)^{\frac{1}{2}} \cdot (\ Q\Delta T^{-\zeta} - 1\ )^{-\frac{1}{2}}. \qquad ...(40)$$

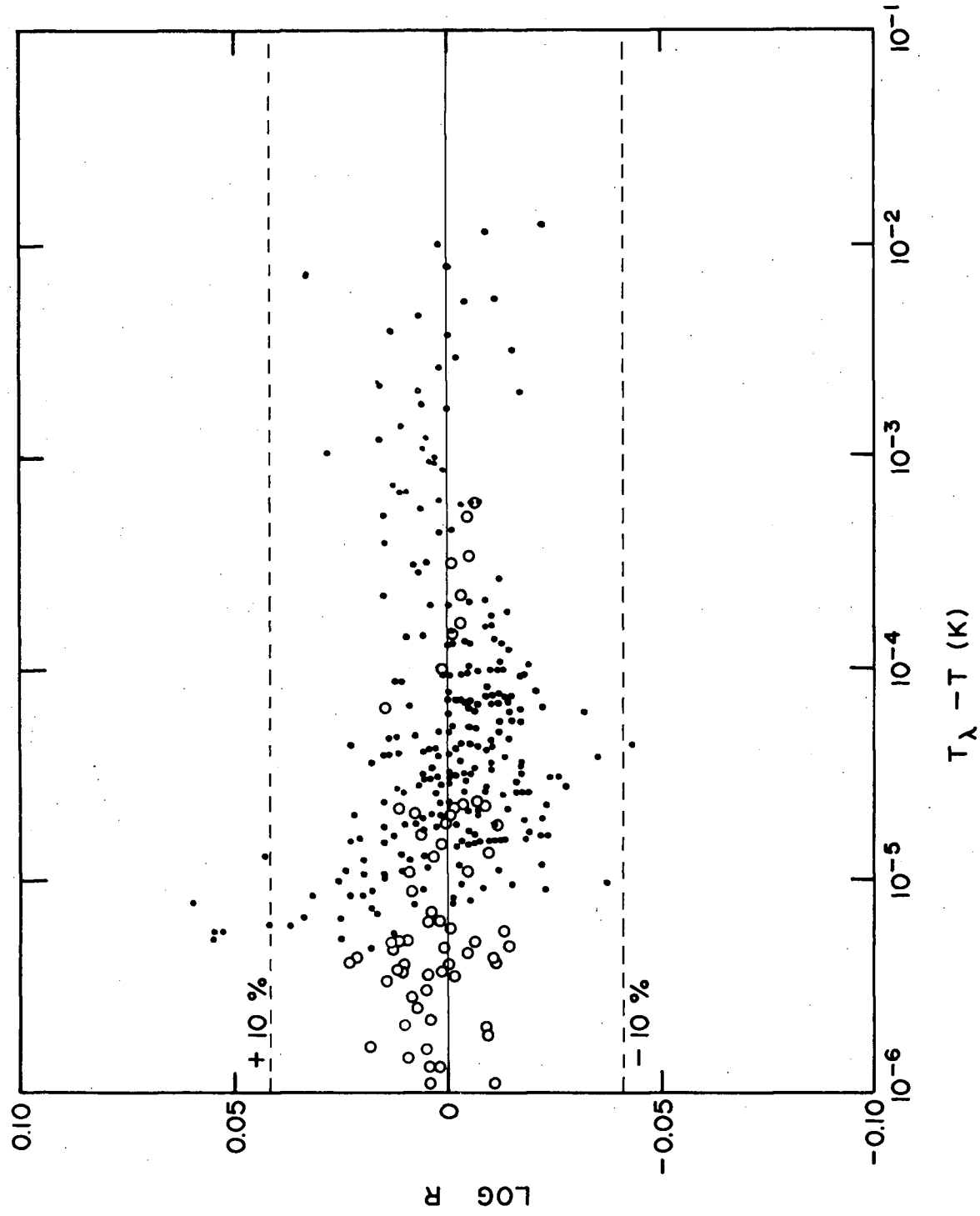

FIGURE 7. Deviation plot comparing the direct measurements, and the calculations from thermal conductivity and scaling to the hydrodynamic velocity. Dots = $R_1 = u_{2e}/u_{2h}$, open circles = $R_2 = u_{2s}/u_{2h}$.

We obtained $Q = 0.67 \pm .02$ and $\zeta = +.671 \pm .004$ (95% confidence limits) in agreement with the more precise values given above in Eq. (33).

(3) COMPARISON WITH THE SCALING PREDICTION.

Recent experimental measurements by Ahlers[17,36] of the thermal conductivity of helium I near the lambda point, combined with our second sound velocity measurements in helium II, make possible a check of the extended dynamic scaling prediction derived above.

Equation (29) may be rewritten

$$K(\Delta T-) = u_2(\Delta T)\rho C_p(\Delta T-)\left\{A\xi_o^2(\xi_o')^{-1}\right\}|\Delta T-|^{-2/3}, \quad \ldots(41)$$

where $\Delta T-$ indicates $T_\lambda - T$ is negative. Substituting for $u_2(\Delta T)$ in Eq. (41) the hydrodynamic velocity $u_{2h}(\Delta T)$, Ahlers performed[17] a least squares fit of the resulting equation to his thermal conductivity measurements, obtaining for the constant

$$A\xi_o^2(\xi_o')^{-1} = (0.87 \pm .06) \times 10^{-8} \text{ cm}. \quad \ldots(42)$$

In performing this fit Ahlers used for $C_p(\Delta T-)$ and $C_p(\Delta T)$, (contained in u_{2h}), his own measurements of C_p.[37] As the ΔT dpendences of Ahlers specific heat and of the BFK specific heat are slightly different, his data are not directly comparable with the hydrodynamic velocities we have calculated. We have therefore repeated the calculations using the BFK specific heat and Ahlers' original thermal conductivity data ($K(\Delta T-)$, $\Delta T-$),[38]

obtaining for the constant

$$A\xi_o^2(\xi_o')^{-1} = (0.86 \pm .06) \times 10^{-8} \text{ cm}, \quad \ldots(43)$$

in agreement with Eq. (42).

Rewriting Eq. (41) we find

$$u_{2s}(\Delta T) = (K(\Delta T-)/\rho C_p(\Delta T-)) \cdot [A\xi_o^2(\xi_o')^{-1}]^{-1} |\Delta T-|^{2/3}, \quad \ldots(44)$$

where the subscript s indicates the velocity is a scaling prediction. For each of the thermal conductivity points $(K(\Delta T-), \Delta T-)$, Eq. (44) was evaluated (with substitution of Eqs. (34) and (43)) and the ratio

$$R_2(\Delta T) \equiv u_{2s}(\Delta T)/u_{2h}(\Delta T)$$

was calculated. The results are shown in Fig. 7. For the 66 points the mean value of R_2 and its 95% confidence limits are

$$\bar{R}_2 = \langle u_{2s}/u_{2h} \rangle_{av} = 1.005 \pm .004 . \quad \ldots(45)$$

CHAPTER VI. CONCLUSIONS AND DISCUSSION.

(1) CONCLUSIONS

The hydrodynamic and the scaling law predictions of the velocity of second sound were tested by comparison with the experimentally determined values. The average value of the ratio of u_{2e} to u_{2h} over the temperature range of the experiment is given by $\bar{R}_1$ in Eq. (39). The equality of $\bar{R}_1$ and unity therefore demonstrates the agreement between the measured velocities and those predicted by two fluid hydrodynamics. Further calculations showed, and Fig. 7 indicates, that within the measured temperature range there were no significant departures of R_1 from unity. In other words, R_1 was observed to be independent of temperature. The hydrodynamic theory therefore appears to properly predict both the magnitude and the temperature dependence of the second sound velocity in the critical region.

A comparison of R_1 with R_2 implies a comparison of u_{2e} and u_{2s} with u_{2h} and hence of u_{2e} with u_{2s}. The equality of $\bar{R}_1$ and $\bar{R}_2$ demonstrates the agreement between the measured velocities and those calculated from dynamic scaling arguements. R_2 was also shown to be independent of temperature. As u_{2s} contains a

constant term (evaluated in Eq. (43)) determined by fitting to the thermal conductivity data, it is this temperature independence of R_2 which constitutes the affirmative test of the scaling law prediction.

On the basis of these results (Eq. (39) and (45)) we conclude that in the critical region for $\Delta T \geq 5 \times 10^{-6}$K the hydrodynamic prediction Eq. (23) and the scaling law prediction Eq. (29) of the velocity of low amplitude, low frequency second sound have been verified.

The verification of the hydrodynamic prediction, and the prediction of the values of Q and ζ in Eq. (40) both imply that the extrapolation of the superfluid density relation Eq. (33) to 5×10^{-6}K was valid.

The experiment also proved that when properly applied, the method of drifting temperatures is well suited for making measurements of physical phenomena near the critical point.

(2) DISCUSSION

In the derivation of Eq. (23) it was assumed explicitly that the velocities $\vec{v}_s$ and $\vec{v}_n$ are small, and implicitly that inhomogeneities (in the absence of second sound) in the thermodynamic properties of the fluid occur only over distances small compared with the second sound wave length (i.e. that $k\xi \ll 1$). In other words,

the derivation was for low amplitude ($\vec{v}_s$ and $\vec{v}_n$ are proportional to the second sound amplitude), low frequency second sound.

In deriving the scaling law prediction, the critical frequency $\omega^q(\vec{k})$ was related (Eq. (25)) to second sound by using the assumption that second sound is the dominant mode of heat transport in Region I (Fig. 1), defined by $k\xi \ll 1$.

Both the above conditions (low velocities, and $k\xi \ll 1$) were met in the experiment, the highest observed second sound amplitude being $\sim 10^{-7}$K RMS, and the largest value of $k\xi$ being ~ 0.02.

A departure from either the low amplitude, or the low frequency condition would presumably be accompanied by a departure of the observed velocity from the hydrodynamic value. Velocities of large amplitude second sound (analogous to shock waves in ordinary sound) different from the hydrodynamic velocity have been observed.[39, 40]

In the critical region very near T_λ the correlation function range ξ is diverging rapidly with decreasing ΔT. It would therefore seem interesting, and not impractical, to make use of higher frequency second sound to enter Region II (Fig. 1) near the critical point

in which $k\xi$ is of the order of, or greater than unity, and in which two fluid hydrodynamics could no longer be presumed valid.

GLOSSARY OF SYMBOLS

A	Constant of order unity.
$\overset{*}{a}$	An operator or physical quantity other than $\overset{*}{p}$.
B_1	Thermometry system sensitivity (ohms per chart division.
C_p	Constant pressure specific heat.
C_v	Constant volume specific heat.
$C^{\overset{*}{a}}$	Correlation function for $\overset{*}{a}$.
$C^{\overset{*}{a}}_f$	Fourier transform of $C^{\overset{*}{a}}$.
C^{aI}, C^{aII}, C^{aIII}	Asymptotic forms of $C^{\overset{*}{a}}_f$ in regions I, II, and III (Fig. 1).
$C^{\overset{*}{b}}$	Correlation function for $\overset{*}{p}$.
d	Resonant cavity spacing.
D_t	Thermal diffusivity.
E	Energy density of the liquid.
$\underline{e}$	A critical exponent.
$\vec{F}$	Entropy flux vector.
f	Second sound frequency.
G	Gibbs free energy per unit mass.
$\vec{j}$	Momentum per unit volume.
k	Wave number.
M	Mass of liquid helium sample.
M_n	Mass of normal fluid component.
M_s	Mass of superfluid component.

n	Resonance mode number. (Equal to the number of half wavelengths of second sound in the cavity).
n'	Relative mode number. Only differences between the n' are correct.
P	Total power dissipation in the cavity.
$\vec{P}_n$	Normal fluid - superfluid relative momentum.
p	Pressure.
p^*	Order parameter.
Q	Coefficient of ΔT in ρ_n/ρ_s expression.
q	Heat operator.
$R(t)$	Thermometer resistance at time t.
R_λ	Electrical resistance of device at T_λ.
S	Entropy per unit mass.
T	Absolute temperature.
T_c	A critical temperature.
T_λ	The lambda temperature 2.172 K.
t	Time.
U	Internal energy per unit mass.
u_1	Velocity of first sound in liquid helium.
u_2	Velocity of second sound in liquid helium.
u_{2e}	u_2 determined experimentally.
u_{2h}	u_2 calculated from hydrodynamics.
u_{2s}	u_2 calculated from thermal conductivity and scaling theory.
V	Specific volume (equal to $1/\rho$).
$\vec{v}_n$	Normal fluid velocity.
$\vec{v}_s$	Superfluid velocity.

W_n	Statistical weight of a data point.
x_k	Cartesian coordinates (k = 1,2,3).
α α' }	Constants of the order of unity.
β	Critical exponent of $\overset{*}{p}$.
Δ_n	A measured distance on a recorder chart. Δ_n is subsequently converted to a temperature difference.
ΔT	$T_\lambda - T$.
$\Delta T'(P)$	T_λ - (the temperature of the sharp discontinuity in the slope of the warming curve).
$\delta(i,k)$	The Kronecker delta function.
ϵ	$(T - T_c)/T_c$.
ζ	Critical exponent of ρ_s.
η	Critical exponent of $C^{\overset{*}{p}}$.
κ	Thermal conductivity.
ν, ν'	Critical exponents of ξ.
ξ	Correlation length, or range of $C^{\overset{*}{p}}$.
Π_{ik}	Momentum flux tensor.
ρ	Density of liquid helium sample.
ρ_n	Density of normal fluid component.
ρ_s	Density of superfluid component.
Σ	$\Sigma = 0$ if $T<T_\lambda$, $\Sigma = 1$ if $T>T_\lambda$.
ω	Angular frequency.
$\omega^{\overset{*}{a}}$	Characteristic frequency for $C_f^{\overset{*}{a}}$.
∇^2	Div grad .

REFERENCES AND FOOTNOTES

1. V.P.Peshkov, Soviet Phys. - JETP, 11, 580 (1960).

2. C.J.Pearce, J.A.Lipa, and M.J.Buckingham, Phys. Rev. Letters, 20, 1471 (1968).

3. J.A.Tyson and D.H.Douglass, Phys. Rev. Letters, 21, 1308 (1968).

4. D.L.Johnson and M.J.Crooks, Phys. Letters, 27A, 688 (1968).

5. A good review of the two fluid model is contained in: J.Wilks, The Properties of Liquid and Solid Helium, (Clarendon Press, Oxford, 1967), Chapter 3.

6. L.D.Landau, J. Phys., Moscow 5, 71 (1941). Reprinted in: I.M.Khalatnikov, Introduction to the Theory of Superfluidity (W.A.Benjamin, Inc. New York, 1965).

7. A good review paper is: L.P.Kadanoff, W.Götze, D.Hamblen, R.Hecht, E.A.S.Lewis, V.V.Palciauskas, M.Rayl, and J.Swift, Rev. Mod. Phys., 39, 395 (1967).

8. M.E.Fisher, J. Math. Phys., 5, 944 (1964).

9. B.Widom, J. Chem. Phys., 43, 3892 (1965), and 43, 3898 (1965).

10. L.P.Kadanoff, Physics, 2, 263 (1966).

11. B.I.Halperin and P.C.Hohenberg, Phys. Rev., 177, 952 (1969).

12. R.A.Ferrell, N.Menyhard, H.Schmidt, F.Schwabl and P.Szepfalusy, (a) Phys. Rev. Letters, 18, 891 (1967), (b) Phys. Letters, 24A, 493 (1967), and (c) Ann. Phys. (N.Y.) , 47, 565 (1968).

13. See Reference 12(c), Equation (5.4).

14. J.R.Clow and J.D.Reppy, Phys.Rev. Letters, 16, 887 (1966).

15. J.A.Tyson and D.H.Douglass, Phys. Rev. Letters, 17, 472 (1966); 17, 622(E) (1966).

16. J.A.Tyson, Phys. Rev., 166, 166 (1968).

17. G.Ahlers, Phys. Rev. Letters, 21, 1159 (1968).

18. E.J.Walker, Rev. Sci. Instr., 30, 834 (1959).

19. CIBA (A.R.L.) Ltd., Duxford, Cambridge, England.

20. G.Ahlers, Phys. Rev., 171, 275 (1968).

21. Princeton Applied Research Corp. Model 122. Typical sensitivity 0.1 to 1.0 mV rms full scale. Typical integration time 1 to 3 seconds.

22. Princeton Applied Research Corp. Model 112 preamplifier. Fixed gain of 40db.

23. Hewlett-Packard / Moseley Division Model 7100B. Typical gain 1 to 5 V full scale.

24. Teltronics Inc. Model CA-2. Typical sensitivity 5 μV rms full scale. Typical integration time 1 second.

25. Tektronix Inc. Model RM 122. Fixed gains of 40db or 60db.

26. W.C.Cannon and M.Chester, Rev. Sci. Instr., 38, 318 (1967).

27. An Introduction to Photofabrication using Kodak Photosensitive Resists, Kodak Publication No. P-79, Eastman Kodak Co., Rochester, N.Y.

28. No. 999 Black. Columbian Carbon Co. of New York, N.Y.

29. Allen-Bradley Co., Milwaukee, Wisconsin.

30. IRC Inc., Boone Division, Boone, North Carolina.

31. Some data were acquired before the neccessity to measure zero-power warming curves was realized. On these early charts, the point A was assumed to be the lambda point. As P was known, these data were subsequently corrected by the addition to their ΔT values of $\Delta T'(P)$ obtained from extrapolation and interpolation of the subsequent measurements of $\Delta T'(P)$ as a fuction of P.

32. Thermal Expansion of Technical Solids at Low Temperatures, National Bureau of Standards Monograph 29, (United States Department of Commerce, Government Printing Office, Washington, D.C., 1961). Note that Perspex and Plexiglass are both manufacturers trade names for polymethylmethacrylate.

33. C.F.Kellers, Thesis, Duke University (1960) unpublished: M.J.Buckingham and W.M.Fairbank, in Progress in Low Temperature Physics, ed. C.J.Gorter (North-Holland Publishing Co.,Amsterdam, 1961), Vol.III, Ch.3.

34. R.W.Hill and O.V.Lounasmaa, Phil. Mag., 2, Ser. 8, 145 (1957).

35. The "correct" weight W_n given to a point should be proportional to the inverse of the variance of that point. The best available estimate of the variance is the square of the probable error. The points were therefore assigned weights W_n proportional to $(2 + 6/\Delta_n)^{-2}$, the number in brackets being the estimated probable fractional error (%) in the measurement of ΔT_n.

36. G.Ahlers, Phys. Letters, 28A, 507 (1969).

37. G.Ahlers, Bull. Am. Phys. Soc., 13, 506 (1968), and to be published.

38. G.Ahlers, private communication.

39. A.J.Dessler and W.M.Fairbank, Phys. Rev., 104, 6 (1956).

40. D.V.Osbourne, Proc. Phys. Soc., A64, 114 (1951).

APPENDIX I

EXPERIMENTAL AND THEORETICAL SECOND SOUND VELOCITIES

TEMPERATURE DIFFERENCE (K)	EXPERIMENTAL VELOCITY (M/SEC)	HYDRODYNAMIC VELOCITY (M/SEC)
4.75E-06	0.335	0.321
5.27E-06	0.353	0.334
5.33E-06	0.380	0.335
5.66E-06	0.389	0.342
5.66E-06	0.353	0.342
5.75E-06	0.389	0.344
5.98E-06	0.342	0.349
6.10E-06	0.383	0.352
6.18E-06	0.389	0.354
6.59E-06	0.383	0.362
6.63E-06	0.392	0.363
6.90E-06	0.383	0.368
7.31E-06	0.392	0.376
7.61E-06	0.389	0.382
7.75E-06	0.383	0.384
7.90E-06	0.444	0.387
7.94E-06	0.383	0.388
8.08E-06	0.389	0.390
8.36E-06	0.425	0.395
8.44E-06	0.415	0.396
8.44E-06	0.418	0.396
8.74E-06	0.418	0.401
8.74E-06	0.418	0.401
8.87E-06	0.383	0.404
8.93E-06	0.410	0.405
9.03E-06	0.399	0.406
9.42E-06	0.399	0.413
9.43E-06	0.410	0.413
9.68E-06	0.383	0.417
9.88E-06	0.446	0.420
1.03E-05	0.441	0.426
1.05E-05	0.444	0.429
1.07E-05	0.453	0.432
1.09E-05	0.446	0.435
1.10E-05	0.425	0.437
1.12E-05	0.465	0.440
1.13E-05	0.446	0.441
1.15E-05	0.441	0.444
1.17E-05	0.425	0.447
1.23E-05	0.465	0.455

TEMPERATURE DIFFERENCE (K)	EXPERIMENTAL VELOCITY (M/SEC)	HYDRODYNAMIC VELOCITY (M/SEC)
1.24E-05	0.478	0.456
1.26E-05	0.465	0.459
1.29E-05	0.511	0.463
1.31E-05	0.478	0.466
1.42E-05	0.478	0.480
1.45E-05	0.478	0.483
1.46E-05	0.478	0.485
1.46E-05	0.478	0.485
1.47E-05	0.479	0.486
1.48E-05	0.504	0.487
1.49E-05	0.480	0.488
1.50E-05	0.486	0.489
1.51E-05	0.480	0.491
1.52E-05	0.478	0.492
1.52E-05	0.479	0.492
1.52E-05	0.486	0.492
1.52E-05	0.519	0.492
1.54E-05	0.480	0.494
1.57E-05	0.478	0.498
1.58E-05	0.523	0.499
1.61E-05	0.517	0.502
1.61E-05	0.478	0.502
1.62E-05	0.478	0.503
1.63E-05	0.498	0.505
1.66E-05	0.486	0.508
1.68E-05	0.504	0.510
1.73E-05	0.523	0.516
1.76E-05	0.523	0.519
1.78E-05	0.540	0.521
1.78E-05	0.519	0.521
1.80E-05	0.536	0.523
1.80E-05	0.536	0.523
1.81E-05	0.511	0.524
1.83E-05	0.536	0.527
1.89E-05	0.511	0.533
1.93E-05	0.510	0.537
1.95E-05	0.547	0.539
2.00E-05	0.547	0.544
2.02E-05	0.574	0.546
2.04E-05	0.553	0.548
2.05E-05	0.540	0.549
2.09E-05	0.547	0.553
2.12E-05	0.547	0.556
2.14E-05	0.540	0.558
2.26E-05	0.540	0.569

TEMPERATURE DIFFERENCE (K)	EXPERIMENTAL VELOCITY (M/SEC)	HYDRODYNAMIC VELOCITY (M/SEC)
2.29E-05	0.574	0.572
2.30E-05	0.574	0.573
2.34E-05	0.597	0.577
2.51E-05	0.574	0.592
2.53E-05	0.597	0.593
2.55E-05	0.574	0.595
2.55E-05	0.589	0.595
2.57E-05	0.574	0.597
2.58E-05	0.574	0.598
2.63E-05	0.618	0.602
2.63E-05	0.589	0.602
2.68E-05	0.623	0.606
2.72E-05	0.597	0.609
2.75E-05	0.574	0.612
2.76E-05	0.622	0.613
2.79E-05	0.618	0.615
2.86E-05	0.598	0.621
2.87E-05	0.622	0.622
2.90E-05	0.618	0.624
2.97E-05	0.638	0.630
2.98E-05	0.638	0.630
2.99E-05	0.639	0.631
3.01E-05	0.638	0.633
3.01E-05	0.598	0.633
3.02E-05	0.599	0.633
3.03E-05	0.638	0.634
3.03E-05	0.598	0.634
3.05E-05	0.599	0.636
3.09E-05	0.638	0.639
3.09E-05	0.639	0.639
3.10E-05	0.648	0.640
3.11E-05	0.638	0.640
3.14E-05	0.618	0.643
3.15E-05	0.639	0.643
3.16E-05	0.638	0.644
3.18E-05	0.638	0.646
3.20E-05	0.648	0.647
3.30E-05	0.639	0.655
3.33E-05	0.648	0.657
3.42E-05	0.670	0.663
3.44E-05	0.639	0.665
3.54E-05	0.656	0.672
3.55E-05	0.646	0.673
3.57E-05	0.702	0.674
3.59E-05	0.670	0.675

TEMPERATURE DIFFERENCE (K)	EXPERIMENTAL VELOCITY (M/SEC)	HYDRODYNAMIC VELOCITY (M/SEC)
3.81E-05	0.670	0.690
3.84E-05	0.638	0.692
3.86E-05	0.718	0.694
3.86E-05	0.697	0.694
3.89E-05	0.718	0.696
3.93E-05	0.697	0.698
3.97E-05	0.721	0.701
4.07E-05	0.717	0.707
4.13E-05	0.697	0.711
4.16E-05	0.721	0.713
4.17E-05	0.718	0.714
4.20E-05	0.712	0.716
4.24E-05	0.706	0.718
4.31E-05	0.706	0.723
4.33E-05	0.656	0.724
4.36E-05	0.765	0.726
4.36E-05	0.765	0.726
4.36E-05	0.718	0.726
4.37E-05	0.721	0.726
4.48E-05	0.717	0.733
4.63E-05	0.767	0.742
4.67E-05	0.721	0.744
4.68E-05	0.765	0.745
4.78E-05	0.765	0.751
4.93E-05	0.738	0.760
4.96E-05	0.765	0.761
4.96E-05	0.765	0.761
4.96E-05	0.765	0.761
5.00E-05	0.765	0.764
5.03E-05	0.765	0.765
5.21E-05	0.765	0.775
5.23E-05	0.767	0.776
5.30E-05	0.778	0.780
5.52E-05	0.765	0.792
5.57E-05	0.765	0.795
5.67E-05	0.778	0.800
6.08E-05	0.820	0.821
6.13E-05	0.765	0.824
6.13E-05	0.797	0.824
6.24E-05	0.797	0.829
6.27E-05	0.820	0.830
6.43E-05	0.797	0.838
6.45E-05	0.830	0.839
6.61E-05	0.865	0.847
6.67E-05	0.836	0.850

TEMPERATURE DIFFERENCE (K)	EXPERIMENTAL VELOCITY (M/SEC)	HYDRODYNAMIC VELOCITY (M/SEC)
6.78E-05	0.836	0.855
6.87E-05	0.850	0.859
6.89E-05	0.852	0.860
6.95E-05	0.842	0.863
6.97E-05	0.862	0.864
6.97E-05	0.836	0.864
7.06E-05	0.865	0.868
7.10E-05	0.865	0.870
7.25E-05	0.850	0.877
7.34E-05	0.862	0.881
7.35E-05	0.852	0.881
7.38E-05	0.861	0.882
7.54E-05	0.865	0.889
7.62E-05	0.893	0.893
7.63E-05	0.852	0.893
8.04E-05	0.893	0.911
8.53E-05	0.957	0.931
8.54E-05	0.957	0.932
8.59E-05	0.957	0.934
9.09E-05	0.918	0.954
9.10E-05	0.957	0.954
9.10E-05	0.957	0.954
9.15E-05	0.957	0.956
9.16E-05	0.957	0.956
9.17E-05	0.918	0.957
9.21E-05	0.957	0.958
9.39E-05	0.959	0.965
9.39E-05	0.957	0.965
9.44E-05	0.959	0.967
9.56E-05	0.957	0.972
9.75E-05	0.957	0.979
9.84E-05	0.957	0.982
9.88E-05	0.957	0.984
1.02E-04	0.985	0.995
1.03E-04	0.957	0.999
1.07E-04	0.985	1.013
1.22E-04	1.030	1.064
1.27E-04	1.081	1.080
1.28E-04	1.081	1.084
1.28E-04	1.052	1.084
1.31E-04	1.081	1.093
1.33E-04	1.090	1.099
1.33E-04	1.090	1.099
1.36E-04	1.081	1.108
1.41E-04	1.150	1.124

TEMPERATURE DIFFERENCE (K)	EXPERIMENTAL VELOCITY (M/SEC)	HYDRODYNAMIC VELOCITY (M/SEC)
1.45E-04	1.150	1.135
1.51E-04	1.149	1.153
1.58E-04	1.148	1.173
1.59E-04	1.149	1.175
1.79E-04	1.200	1.229
1.83E-04	1.200	1.239
1.99E-04	1.290	1.279
1.99E-04	1.280	1.279
1.99E-04	1.280	1.279
2.06E-04	1.279	1.295
2.11E-04	1.279	1.307
2.22E-04	1.379	1.332
2.62E-04	1.379	1.418
2.82E-04	1.480	1.458
3.06E-04	1.530	1.503
3.11E-04	1.530	1.512
3.98E-04	1.720	1.660
4.35E-04	1.724	1.717
4.43E-04	1.724	1.729
5.27E-04	1.910	1.846
5.57E-04	1.910	1.885
5.88E-04	1.913	1.924
6.01E-04	1.913	1.941
6.05E-04	1.913	1.945
6.11E-04	1.960	1.953
6.62E-04	2.060	2.014
6.64E-04	2.070	2.017
7.25E-04	2.150	2.085
8.70E-04	2.240	2.235
9.15E-04	2.300	2.278
9.22E-04	2.300	2.285
9.74E-04	2.350	2.333
1.03E-03	2.540	2.382
1.08E-03	2.460	2.426
1.20E-03	2.620	2.525
1.23E-03	2.580	2.549
1.39E-03	2.740	2.671
1.67E-03	2.870	2.866
1.75E-03	2.960	2.918
2.01E-03	2.960	3.077
2.03E-03	3.140	3.089
2.17E-03	3.290	3.174
2.65E-03	3.440	3.426
2.65E-03	3.440	3.426
2.95E-03	3.550	3.570

TEMPERATURE DIFFERENCE (K)	EXPERIMENTAL VELOCITY (M/SEC)	HYDRODYNAMIC VELOCITY (M/SEC)
3.18E-03	3.550	3.674
3.74E-03	3.920	3.914
3.93E-03	4.110	3.989
4.62E-03	4.310	4.244
5.32E-03	4.440	4.482
5.53E-03	4.440	4.549
7.35E-03	5.480	5.079
7.90E-03	5.230	5.222
9.99E-03	5.740	5.715
1.15E-02	5.920	6.042
1.25E-02	5.920	6.233